Journal of Materials Science & Technology 77 (2021) 223–236

Contents lists available at ScienceDirect

Journal of Materials Science & Technology

journal homepage: www.jmst.org

Research Article

Effects of intermittent loading time and stress ratio on dwell fatigue behavior of titanium alloy Ti-6Al-4V ELI used in deep-sea submersibles

Chengqi Sun[a,b,*], Yanqing Li[c], Kuilong Xu[d], Baotong Xu[e]

[a] State Key Laboratory of Nonlinear Mechanics, Institute of Mechanics, Chinese Academy of Sciences, Beijing, 100190, China
[b] School of Engineering Sciences, University of Chinese Academy of Sciences, Beijing 100049, China
[c] State Key Laboratory of Deep-sea Manned Vehicles (China Ship Scientific Research Center), Wuxi 214082, China
[d] Luoyang Ship Material Research Institute, Luoyang, 471023, China
[e] Aero Engine Corporation of China Beijing Institute of Aeronautical Materials, Beijing 100095, China

ARTICLE INFO

Article history:
Received 30 August 2020
Received in revised form 19 October 2020
Accepted 21 October 2020
Available online 20 November 2020

Keywords:
Ti-6Al-4V ELI
Dwell fatigue
Intermittent loading time
Stress ratio
Creep fatigue interaction

ABSTRACT

Different components of deep-sea submersibles, such as the pressure hull, are usually subjected to intermittent loading, dwell loading, and unloading during service. Therefore, for the design and reliability assessment of structural parts under dwell fatigue loading, understanding the effects of intermittent loading time on dwell fatigue behavior of the alloys is essential. In this study, the effects of the intermittent loading time and stress ratio on dwell fatigue behavior of the titanium alloy Ti-6Al-4 V ELI were investigated. Results suggest that the dwell fatigue failure modes of Ti-6Al-4 V ELI can be classified into three types, i.e., fatigue failure mode, ductile failure mode, and mixed failure mode. The intermittent loading time does not affect the dwell fatigue behavior, whereas the stress ratio significantly affects the dwell fatigue life and dwell fatigue mechanism. The dwell fatigue life increases with an increase in the stress ratio for the same maximum stress, and specimens with a negative stress ratio tend to undergo ductile failure. The mechanism of dwell fatigue of titanium alloys is attribute to an increase in the plastic strain caused by the part of the dwell loading, thereby resulting in an increase in the actual stress of the specimens during the subsequent loading cycles and aiding the growth of the formed crack or damage, along with the local plastic strain or damage induced by the part of the fatigue load promoting the cumulative plastic strain during the dwell fatigue process. The interaction between dwell loading and fatigue loading accelerates specimen failure, in contrast to the case for individual creep or fatigue loading alone. The dwell fatigue life and cumulative maximum strain during the first loading cycle could be correlated by a linear relationship on the log–log scale. This relationship can be used to evaluate the dwell fatigue life of Ti alloys with the maximum stress dwell.

1. Introduction

Deep sea contains biological and mineral resources in large amounts. However, the development of deep-sea submersibles is one of the primary bottlenecks that limits the scientific research and resource development in this field. The key of deep-sea submersibles in service and safety is the reliability of their pressure hull, which is subjected to dwell fatigue loading owing to the changes in the seawater pressure during their service life. Titanium alloys are suitable for the pressure hull structure of submersibles owing to their high strength, low density, and high corrosion resistance. Therefore, it is essential to investigate the dwell fatigue behavior of titanium alloys.

Investigations of the dwell fatigue of titanium alloys can be traced to the early 1970s, when the in-service failure was first reported in the fan discs of the Rolls-Royce RB211 engine on the Lockheed Tristar aircraft [1,2]. Subsequently, the dwell fatigue of titanium alloys has drawn great attention [3–8]. For instance, it has been shown that the dwell of maximum stress can significantly reduce the fatigue life of titanium alloys [9–11] and increase the crack growth rate [12–15]. Moreover, the crack initiation sites

* Corresponding author at: State Key Laboratory of Nonlinear Mechanics, Institute of Mechanics, Chinese Academy of Sciences, Beijing, 100190, China.
E-mail address: scq@lnm.imech.ac.cn (C. Sun).

https://doi.org/10.1016/j.jmst.2020.10.063
1005-0302/

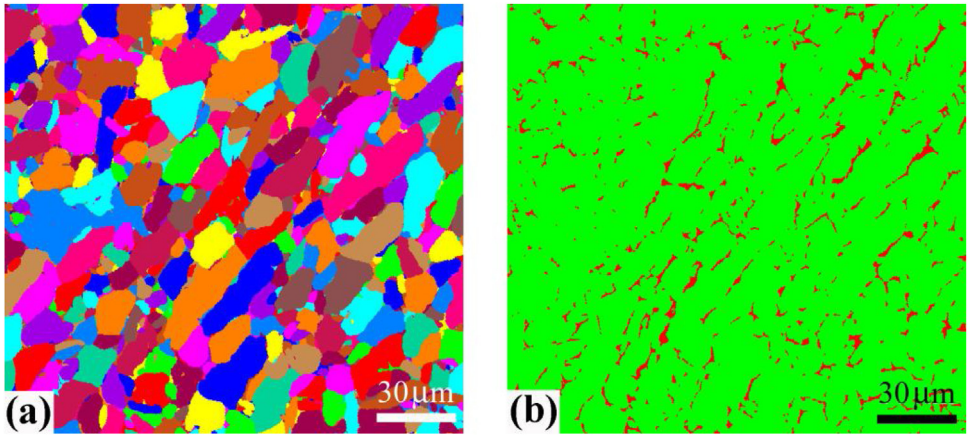

Fig. 1. Microstructures in the transverse section of specimens. (a) EBSD grain map and (b) EBSD phase map corresponding to (a); α- and β-phase are denoted in green and red, respectively.

often exhibit cleavage or quasicleavage facets for titanium alloys subjected to dwell fatigue [2,9,16,17]. Investigations based on the near-α titanium alloys IMI685 [18], IMI834 [10], and Ti60 [19] have shown that the facet surface is usually approximately perpendicular to the tensile stress axis. It has also been shown that the microstructure [10,20], stress ratio [10], temperature [21], and hydrogen concentration [22,23] have a determining effect on the dwell fatigue behavior of titanium alloys. For example, a decrease in the volume fraction of the primary α-phase increases the dwell fatigue life of the Ti60 alloy [24]. The dwell fatigue life of near-α titanium alloy IMI834 at positive stress ratios is lower than that at negative stress ratios [10].

Submersibles experience discontinuous loading (dive), dwell loading (work), and unloading (float) during operation. This corresponds to a period of zero loading (i.e., an intermittent loading time) during the dwell fatigue loading. To evaluate the safety of the structural parts of deep-sea submersibles under dwell fatigue loading, the effect of intermittent loading time on dwell fatigue mechanism of titanium alloys and how does the intermittent loading time affect the dwell fatigue life should be investigated. However, to the best of our knowledge, there have been no studies on these topics, although the fatigue behavior of metallic materials has been investigated widely [25–28].

This work aims to elucidate the effects of intermittent loading time and stress ratio on the dwell fatigue behavior of the Ti-6Al-4 V ELI alloy, which is used for the pressure hull of deep-sea submersibles. The characteristic of the fracture surface is investigated based on the observation by a scanning electron microscopy (SEM). Moreover, the creep behavior and the effect of prior creep on the fatigue behavior are studied. The interaction between dwell loading (i.e., creep) and fatigue loading is also discussed based on the experimental results.

2. Materials and methods

2.1. Materials

Herein, we used the Ti-6Al-4 V ELI alloy. The test specimens were cut from a forged then rolled plate parallel to the rolling direction. The chemical composition (wt.%) of the alloy was 6.45 Al, 4.08 V, 0.19 Fe, 0.0055 C, 0.0033 H, 0.11 O, and Ti (Bal.). The microstructure of the material consisted of an approximately equiaxed α-phase and lamellar β_{tran}, with a certain elongation in the sections perpendicular to the rolling plane. The microstructure in the transverse section of specimens is shown in Fig. 1. The average tensile strength and yield strength of the three tested specimens were 933 and 853 MPa, respectively.

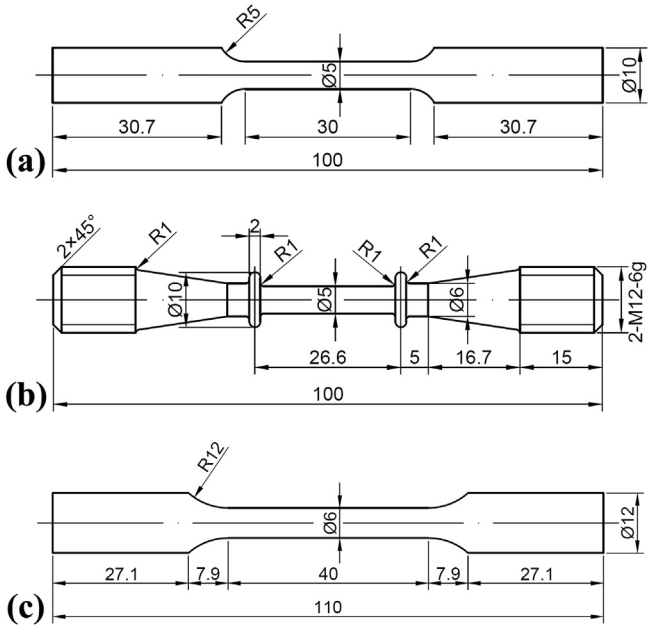

Fig. 2. Shapes and dimensions of specimens (in mm) for (a) tensile test, (b) creep test, and (c) conventional fatigue test and dwell fatigue test at stress ratio $R = 0$.

2.2. Test methods

To investigate the dwell loading (creep)–fatigue interaction and the effects of intermittent loading time and stress ratio on the dwell fatigue behavior of the Ti-6Al-4 V ELI alloy, the following tests were performed:

2.2.1. Tensile test

The tensile tests were performed on specimens (Fig. 2(a)) using an Instron machine to obtain the stress–strain curves.

2.2.2. Tensile test after dwell loading

To evaluate the effect of prior dwell loading (i.e., prior creep) on the tensile strength and yield strength of the material, a constant tensile load was first applied to test specimens of the same size as those corresponding to Fig. 2(a) using a QBR-30 J machine except that a screw thread was formed at the two ends of the specimens.

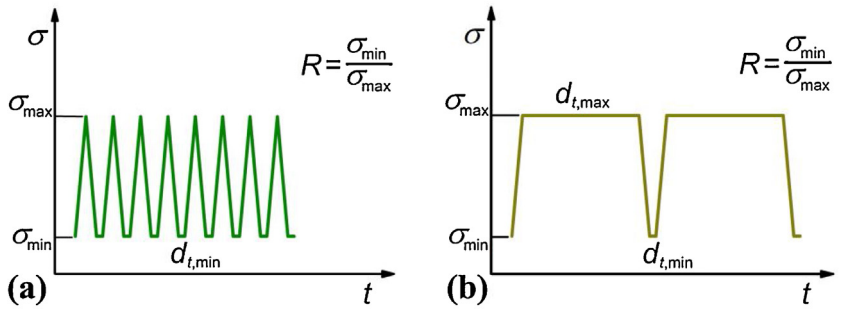

Fig. 3. Schematics of loading waveforms. (a) Conventional fatigue test performed using continuous triangular wave ($d_{t,\min} = 0$) or intermittent triangular wave ($d_{t,\min} > 0$); (b) Dwell fatigue test performed using continuous trapezoidal wave ($d_{t,\min} = 0$) or intermittent trapezoidal wave ($d_{t,\min} > 0$).

Subsequently, the specimens were subjected to tensile tests. The stress during the tensile tests was calculated based on the diameter of test section of the specimens after they had been subjected to prior creep.

2.2.3. Tensile test after fatigue loading

To elucidate the effect of prior fatigue loading on the tensile strength and yield strength of the material, the test specimen (Fig. 2(c)) was at first subjected to fatigue loading for a number of cycles using a MTS Landmark machine. The fatigue loading was performed in the load control mode. The loading waveform was a continuous triangular wave, as shown in Fig. 3(a). The maximum and minimum stresses for the fatigue loading process were calculated based on the initial diameter of the test section of specimen. The stress for the tensile test of the specimen subjected to prior fatigue loading was calculated based on the diameter of the test section after the prior fatigue loading process.

2.2.4. Creep test

The creep tests were conducted on the test specimens (Fig. 2(b)) using a QBR-30 J machine to determine the variations in the strain with dwell loading time (i.e., creep time) under a constant tensile load.

2.2.5. Dwell fatigue test

The dwell fatigue tests were performed with the MTS Landmark machine, and the strain during the tests was measured with an extensometer. The dwell fatigue loading was performed in the load control mode. The maximum and minimum stresses were calculated based on the initial diameter of the test section of specimens. A continuous trapezoid wave and intermittent trapezoid wave (Fig. 3(b)) were used to investigate the effects of intermittent loading time on the dwell fatigue behavior. The specimens used for the dwell fatigue tests performed at the stress ratio $R = 0$ are shown in Fig. 2(c). For the dwell fatigue tests performed at negative stress ratios, the specimens were of the same size as that shown in Fig. 2(c) except that the test section was reduced to 15 mm from 40 mm.

2.2.6. Conventional fatigue test

The conventional fatigue tests were performed (Fig. 2(c)) using the MTS Landmark machine, and the strain during the fatigue tests was measured with an extensometer. The fatigue loading mode used was load control. The maximum and minimum stresses were calculated based on the initial diameter of the test section of specimens. A continuous triangular wave and intermittent triangular wave (Fig. 3(a)) were used to investigate the effect of intermittent loading time on the conventional fatigue behavior.

2.2.7. Fatigue test after dwell loading

To evaluate the effect of prior dwell loading (i.e., prior creep) on the fatigue behavior of the material, several specimens were at first subjected to a constant tensile load using either the MTS Landmark machine or the QBR-30 J machine. The specimens subjected to prior-creep loading using the MTS Landmark machine are shown in Fig. 2. The strain during the tests was measured using an extensometer. The specimens subjected to prior-creep loading using the QBR-30 J machine were similar to that shown in Fig. 2(c); the difference was that a screw thread was formed at their two ends. Then, conventional fatigue tests were performed on these specimens using the MTS Landmark machine, and the strain during the tests was measured with an extensometer. The fatigue loading mode was load control. The loading waveform was a continuous triangular wave, as shown in Fig. 3(a).

The rise time and the fall time are both 2 s for the dwell fatigue tests and conventional fatigue tests. All the tests were performed at room temperature in air. Before the tests, the test surfaces of the specimens were ground and polished to eliminate the machine-generated scratches. The fracture surfaces of the failed specimens were observed using a scanning electron microscopy (SEM) system.

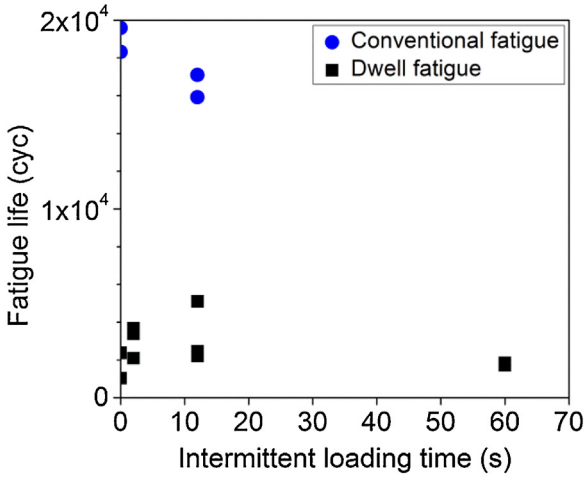

Fig. 4. Variations in dwell fatigue life and conventional fatigue life with intermittent loading time.

3. Results and analysis

3.1. Effect of intermittent loading time on dwell fatigue and conventional fatigue behavior

3.1.1. Fatigue life

Fig. 4 shows the effect of intermittent loading time on dwell fatigue life, which is compared with the effect of that on the conventional fatigue life. The loading information and associated fatigue life data are shown in Table 1. Fig. 4 indicates that the intermittent loading time generally has no effect on the dwell fatigue life

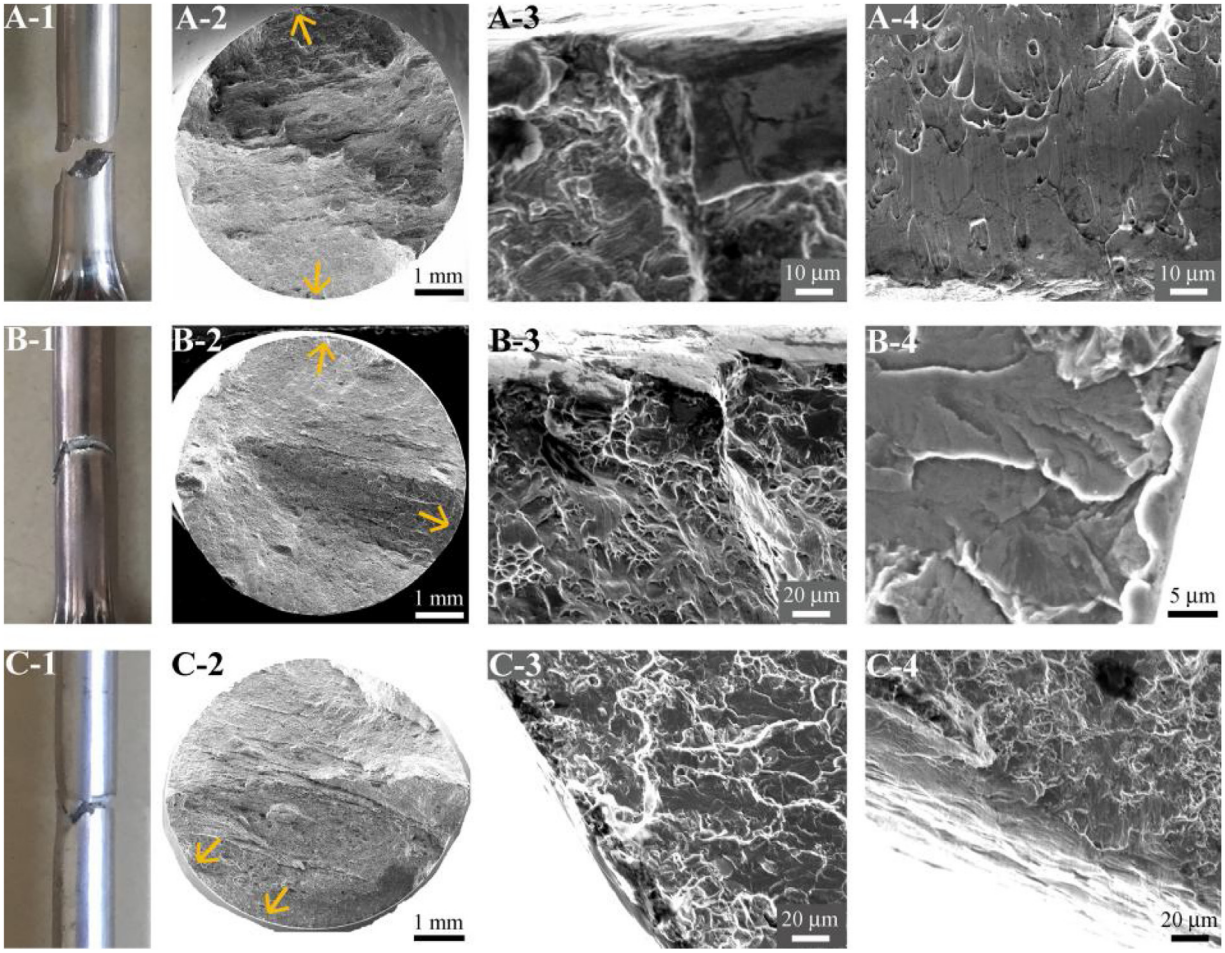

Fig. 5. Photographs and fracture surface morphologies of failed specimens subjected to dwell fatigue tests at σ_{max}=815 MPa, $d_{t,max}$ = 120 s, σ_{min}=0 MPa, and $d_{t,min}$ = 0 s. A-1 to A-4: N_f = 2373 cycles; A-1 is photograph of fractured specimen, A-2 is SEM image of fracture surface, and A-3 and A-4 are magnified images of regions corresponding to up and down arrows in A-2, respectively. B-1 to B-4: N_f = 2384 cycles, B-1 is photograph of fractured specimen, B-2 is SEM image of fracture surface, and B-3 and B-4 are magnified images of regions corresponding to up and right arrows in B-2, respectively. C-1 to C-4: N_f = 1028 cycles; C-1 is photograph of fractured specimen, C-2 is SEM image of fracture surface, and C-3 and C-4 are magnified images of regions corresponding to lower left and down arrows in C-2, respectively.

Table 1
Loading information and associated fatigue life and failure mode data for specimens in Fig. 4.

Maximum stress (MPa)	Dwell time $d_{t,max}$ (s)	Minimum stress (MPa)	Intermittent loading time $d_{t,min}$ (s)	Stress ratio, R	Fatigue life (cyc)	Failure mode
815	120	0	0	0	2373	Fatigue
815	120	0	0	0	2384	Mixed
815	120	0	0	0	1028	Mixed
815	120	0	2	0	3669	Ductile
815	120	0	2	0	3391	Fatigue
815	120	0	2	0	2099	Mixed
815	120	0	12	0	5096	Ductile
815	120	0	12	0	2198	Mixed
815	120	0	12	0	2456	Mixed
815	120	0	60	0	1844	Mixed
815	120	0	60	0	1714	Mixed
815	0	0	0	0	18,317	Fatigue
815	0	0	0	0	19,585	Fatigue
815	0	0	12	0	15,920	Fatigue
815	0	0	12	0	17,098	Fatigue

in the view of all the tested intermittent loading time although the scatter of the fatigue life at the intermittent loading time 12 s is a little bigger than those at the intermittent loading time 0 s, 2 s and 60 s. While the intermittent loading time decreases the conventional fatigue life, and the dwell loading significantly decreases the fatigue life for both the intermittent and continuous fatigue test.

3.1.2. Fracture surface morphology after dwell fatigue loading

SEM observations indicated that the fracture surfaces of the Ti-6Al-4 V ELI alloy specimens exhibited different characteristics during the dwell fatigue tests. Based on the fracture surface characteristics, the failure modes could be classified into three types:

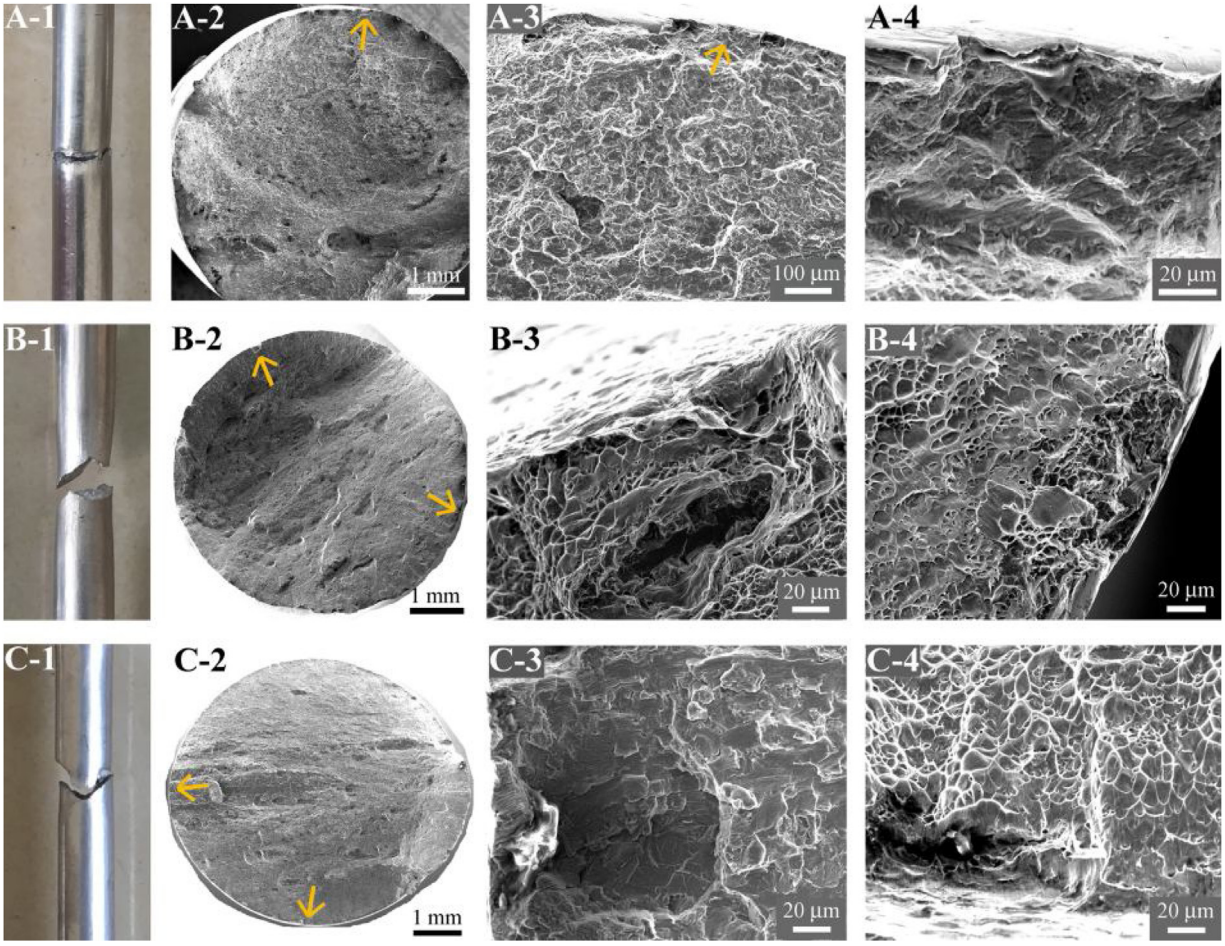

Fig. 6. Photographs and fracture surface morphologies of failed specimens subjected to dwell fatigue tests at σ_{max}=815 MPa, $d_{t,max}$ = 120 s, σ_{min}=0 MPa, and $d_{t,min}$ = 2 s. A-1 to A-4: N_f = 3391 cycles, A-1 is photograph of fractured specimen, A-2 is SEM image of fracture surface, and A-3 and A-4 are magnified images of regions corresponding to arrows in A-2 and A-3, respectively. B-1 to B-4: N_f = 3669 cycles, B-1 is photograph of fractured specimen, B-2 is SEM image of fracture surface, and B-3 and B-4 are magnified images of regions corresponding to up and right arrows in B-2, respectively. C-1 to C-4: N_f = 2099 cycles; C-1 is photograph of fractured specimen, C-2 is SEM image of fracture surface, and C-3 and C-4 are magnified images of regions corresponding to down and left arrows in C-2, respectively.

3.1.2.1. Fatigue failure mode. These specimens exhibited fatigue failure features on their fracture surfaces (A-2 and A-3 in Fig. 5 and A-2 to A-4 in Fig. 6). They did not show necking phenomenon close to the fracture position (A-1 in Figs. 5 and 6).

3.1.2.2. Ductile failure mode. These specimens exhibited dimple-like features on their fracture surfaces (B-2 to B-4 in Figs. 6 and 7) although there might be small local regions of crack initiation and crack growth at and near the specimen surfaces (B-4 in Fig. 6), in contrast to the case for the specimens that exhibited fatigue failure. Further, similar to the case for the specimens subjected to the conventional tensile test (D-2 to D-4 in Fig. 7), the specimens that exhibited the ductile failure mode exhibited necking phenomenon close to the fracture position (B-1 in Figs. 6 and 7), as that observed for the conventional fatigue of Ti-6Al-4 V alloy at high stress ratios [29].

3.1.2.3. Mixed failure mode. These specimens exhibited fatigue crack initiation and growth in some regions of their fracture surfaces (B-2, B-4, C-2 and C-3 in Fig. 5; C-2 and C-3 in Figs. 6 and 7; and B-2 and B-3 in Fig. 8). However, the fracturing of these specimens was due to both fatigue cracks and plastic deformation (B-2 to B-4 and C-2 to C-4 in Fig. 5; C-2 to C-4 in Figs. 6 and 7; and B-2 to B-4 in Fig. 8). Some of these specimens exhibited fatigue-failure-like features. However, the grains in the crack initiation and growth regions exhibited relatively greater deformation (A-2 to A-4 in Figs. 7 and 8). In the case of the mixed failure mode, the specimens did not exhibit necking phenomenon close to the fracture position (B-1 and C-1 in Fig. 5; C-1 in Fig. 6, A-1 and C-1 in Fig. 7; and A-1 and B-1 in Fig. 8).

As listed in Table 1, specimens that subjected to continuous loading exhibited fatigue failure (A-2 to A-4 in Fig. 5) and mixed failure (B-2 to B-4 and C-2 to C-4 in Fig. 5). The specimens subjected to an intermittent loading time of 2 s exhibited fatigue failure (A-2 to A-4 in Fig. 6), ductile failure (B-2 to B-4 in Fig. 6), and mixed failure (C-2 to C-4 in Fig. 6). The specimens subjected to an intermittent loading time of 12 s exhibited ductile failure (B-2 to B-4 in Fig. 7) and mixed failure (A-2 to A-4 and C-2 to C-4 in Fig. 7). The specimens subjected to an intermittent loading time of 60 s exhibited mixed failure (A-2 to A-4 and B-2 to B-4 in Fig. 8). Therefore, it can be concluded that the intermittent loading time has no effect on the dwell fatigue mechanism of the Ti-6Al-4 V ELI alloy. Furthermore, it was found that the dwell fatigue life is related to the failure mode. The specimens that exhibited the ductile failure mode showed longer dwell fatigue lives than those of the specimens that showed the fatigue failure and mixed failure modes.

In addition, the crack initiation sites in titanium alloys often exhibit facets under dwell fatigue loading [2,9,16,17]. In the case of the Ti-6Al-4 V ELI alloy, no facets were observed in the crack initiation regions of the specimens that showed the fatigue failure mode. However, for the specimens that showed the mixed failure

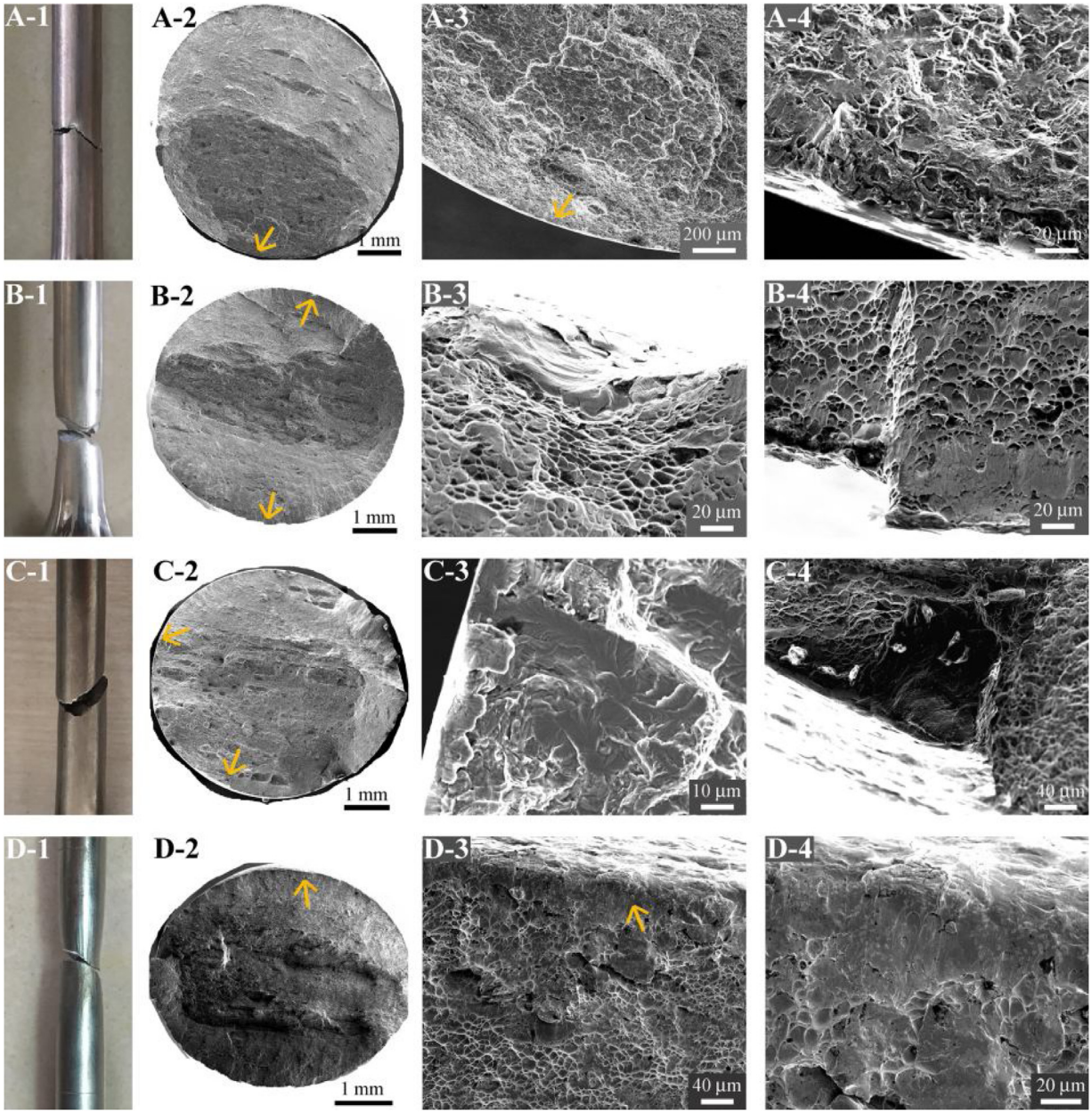

Fig. 7. Photographs and fracture surface morphologies of failed specimens subjected to dwell fatigue test and tensile test. A-1 to A-4, B-1 to B-4, and C-1 to C-4: specimens subjected to dwell fatigue test, σ_{max}=815 MPa, $d_{t,max}$ = 120 s, σ_{min}=0 MPa, and $d_{t,min}$ = 12 s. A-1 to A-4: N_f = 2198 cycles; A-1 is photograph of fractured specimen, A-2 is SEM image of fracture surface, and A-3 and A-4 are magnified images of regions corresponding to arrows in A-2 and A-3, respectively; B-1 to B-4: N_f = 5096 cycles; B-1 is photograph of fractured specimen, B-2 is SEM picture of fracture surface, and B-3 and B-4 are magnified images of regions corresponding to up and down arrows in B-2, respectively. C-1 to C-4: N_f = 2456 cycles, C-1 is photograph of fractured specimen, C-2 is SEM image of fracture surface, and C-3 and C-4 are magnified images of regions corresponding to down and left arrows in C-2, respectively. D-1 to D-4: tensile specimen, D-1 is SEM image of fracture surface, D-2 is SEM image of fracture surface, and D-3 and D-4 are magnified images of regions corresponding to arrows in D-2 and D-3, respectively.

mode, facets were observed in the crack initiation region (B-4 in Fig. 5, C-3 in Fig. 7, and B-3 in Fig. 8).

3.1.3. *Fracture surface morphology after conventional fatigue loading*

With respect to conventional fatigue loading, all the specimens exhibited the fatigue failure mode, and facets were observed in the crack initiation region. This was true for both the continuous fatigue loading and the fatigue loading with an intermittent loading time of 12 s (A-3, B-3, C-2, C-3, D-2 and D-3 in Fig. 9). This indicates that dwell loading has a significant effect on the crack initiation mechanism of the Ti-6Al-4 V ELI alloy.

In addition, the two specimens subjected to the conventional fatigue test with an intermittent loading time of 12 s exhibited multiple crack initiation sites (C-1 and D-1 in Fig. 9). In contrast, one of the two specimens subjected to the conventional fatigue test without an intermittent loading time exhibited a single crack initiation site (B-1 in Fig. 9). The other exhibited multiple crack initiation sites, however, one of the crack regions is very small (A-1 to A-3 in Fig. 9). This indicates that the intermittent loading time tends to induce multiple crack initiation during conventional fatigue loading. This may be the reason that the intermittent loading time decreasing the conventional fatigue life of the investigated Ti-6Al-4 V ELI alloy.

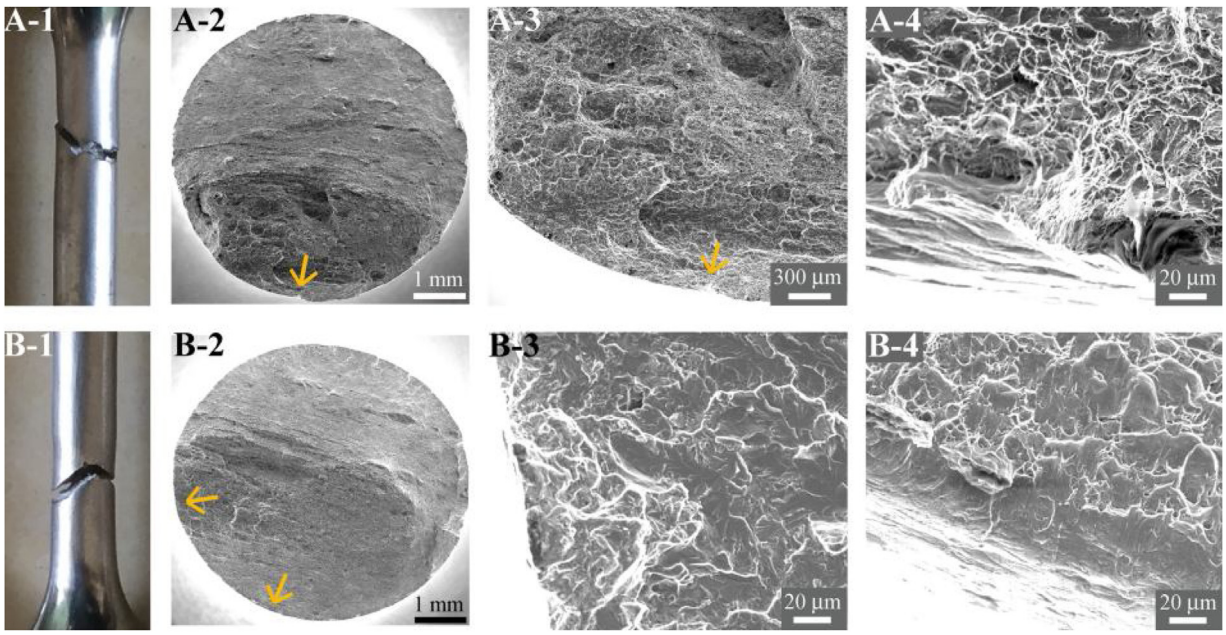

Fig. 8. Photographs and fracture surface morphologies of failed specimens subjected to dwell fatigue tests at σ_{max}=815 MPa, $d_{t,max}$ = 120 s, σ_{min}=0 MPa, and $d_{t,min}$ = 60 s. A-1 to A-4: N_f = 1844 cycles; A-1 is photograph of fracture specimen, A-2 is SEM image of fracture surface, and A-3 and A-4 are magnified images of regions corresponding to arrows in A-2 and A-3, respectively. B-1 to B-4: N_f = 1714 cycles; B-1 is photograph of fractured specimen, B-2 is SEM image of fracture surface, and B-3 and B-4 are magnified images of regions corresponding to left and down arrows in B-2, respectively.

3.1.4. Variations in cumulative strain with loading cycles

Fig. 10 shows the variations in cumulative maximum and minimum strains with the number of loading cycles for the specimens fractured within the extensometer during the dwell fatigue test. It can be seen that the cumulative maximum and minimum strains both increase with an increase in the number of loading cycles and that the cumulative maximum strain increases suddenly when the specimen fails. When combined with the SEM images showing the fracture surface morphologies in Figs. 5–7, these results suggest that the cumulative maximum and minimum strains of the specimens that exhibit ductile failure (which corresponds to the maximum fatigue life in Fig. 10) increase faster than those of the specimens that exhibit fatigue failure or mixed failure (the other specimens in Fig. 10) close to the point of fracture. This indicates that the variation in cumulative strain with the number of loading cycles is related to the failure mode of the specimens during the dwell fatigue process. Fig. 10 also shows that there is no obvious relationship between the dwell fatigue life and cumulative maximum strain just before specimen failure.

3.2. Effect of stress ratio on dwell fatigue behavior

3.2.1. Fatigue life

Fig. 11 shows the dwell fatigue life at different stress ratios *R*. The loading information and associated fatigue life data for the negative stress ratios are shown in Table 2. It can be seen from Fig. 11(a) that for the same maximum stress, the dwell fatigue life increases with an increase in the stress ratio. This result is in contrast to the effect of *R* on the dwell fatigue life of the near-α Ti alloy IMI834, whose dwell fatigue life for positive stress ratios is lower than that for negative stress ratios [10].

Further, it was found that the dwell fatigue life on the logarithmic scale and stress ratio exhibit a linear relationship, as shown in Fig. 11(a). The correlation coefficient was 0.951, indicating that the correlation was highly significant [30]. It was also found that the fatigue life on the logarithmic scale is proportional to (1–*R*)/2 on the logarithmic scale, as shown in Fig. 11(b). The correlation coefficient was –0.944, indicating that the correlation is highly significant [30].

3.2.2. Fracture surface morphology

SEM observations indicated that for negative stress ratios, all the specimens exhibited ductile failure when subjected to dwell fatigue. Photographs of the fractured specimens and their fracture surface morphologies at stress ratios *R* of –1 and –0.5 are shown in Fig. 12. A comparison with the failure mode at *R* = 0 showed that the stress ratio has an effect on the dwell fatigue mechanism. For negative stress ratios, the specimens tend to exhibit ductile failure. In addition, images A-1 to C-1 in Fig. 12 show that the necking is more pronounced at *R* = –1 than *R* = –0.5.

3.2.3. Variations in cumulative strain with loading cycles

Fig. 13 shows the variations in cumulative maximum and minimum strains with loading cycles for the dwell-fatigued specimens fractured within the extensometer at different stress ratios. It can be seen that the cumulative strain increases with the number of loading cycles, and this is true for all the stress ratios (–1, –0.5, and 0). A higher stress ratio results in greater cumulative maximum and minimum strains in the initial stage of loading. As the number of cycles is increased and the specimen is close to the point of fracture, the cumulative maximum strain for the negative stress ratios increases faster than that for *R* = 0. This result agrees with the fracture surface morphologies of the specimens in Figs. 5 and 12 that all the specimens at *R* = –1 and –0.5 exhibited ductile failure while the specimen at *R* = 0 underwent mixed failure.

4. Discussion

4.1. Effects of prior creep and fatigue loading on tensile behavior

Fig. 14 shows the effects of prior creep and fatigue loading on the tensile behavior of the alloy. The steps in the curves are attributable to the unloading related to the removal of the extensometer and subsequent reloading. For the specimens subjected to prior creep or fatigue loading, their diameters after the process were used

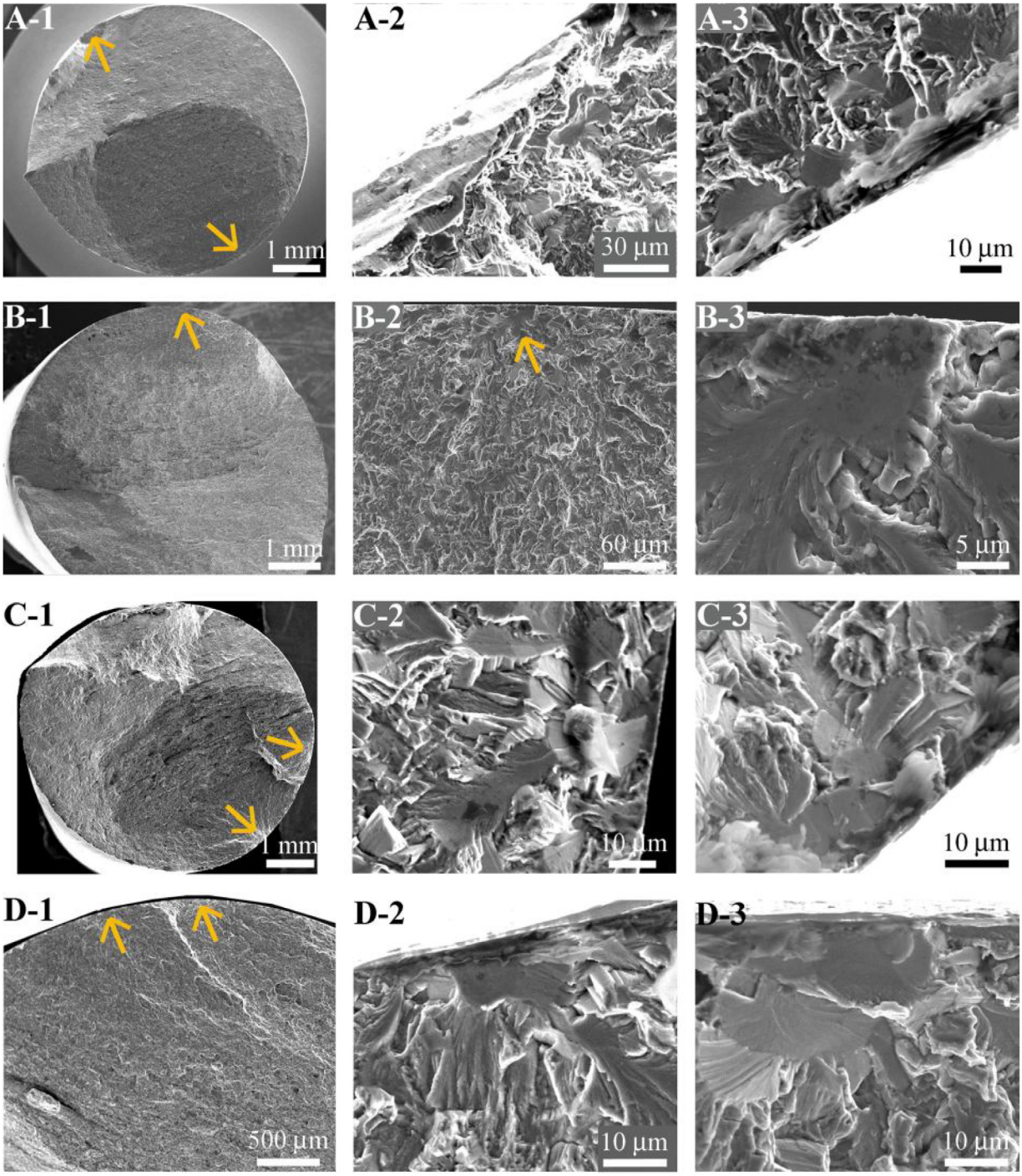

Fig. 9. Fracture surface morphologies of failed specimens subjected to conventional fatigue test and intermittent conventional fatigue test. A-1 to A-3 and B-1 to B-3: specimens subjected to conventional fatigue test, σ_{max}=815 MPa and σ_{min}=0 MPa. A-1 to A-3: N_f = 18,317 cycles; A-1 is SEM image of fracture surface, and A-2 and A-3 are magnified images of regions corresponding to up and down arrows in A-1, respectively; B-1 to B-3: N_f = 19,585 cycles; B-1 is SEM image of fracture surface, and B-2 and B-3 are magnified images of regions corresponding to arrows in B-1 and B-2, respectively. C-1 to C-3 and D-1 to D-3: Specimens subjected to intermittent conventional fatigue test, σ_{max}=815 MPa, σ_{min}=0 MPa, and $d_{t,min}$ = 12 s; C-1 to C-3: N_f = 15,920 cycles; C-1 is SEM image of fracture surface, and C-2 and C-3 are magnified images of regions corresponding to right and lower-right arrows in C-1, respectively; D-1 to D-3: N_f = 17,098 cycles; D-1 is SEM image of fracture surface, and D-2 and D-3 are magnified images of regions corresponding to left and right arrows in D-1, respectively.

Table 2
Loading information and associated fatigue life data for negative stress ratios shown in Fig. 11.

Maximum stress (MPa)	Dwell time $d_{t,max}$ (s)	Minimum stress (MPa)	Intermittent loading time $d_{t,min}$ (s)	Stress ratio R	Fatigue life (cyc)
815	120	−815	0	−1	207
815	120	−815	0	−1	269
815	120	−407.5	0	−0.5	761

Table 3
Tensile strength and yield strength for specimens after being subjected to prior creep or fatigue loading.

Loading type	Tensile strength (MPa)	Yield strength (MPa)
Tensile	930	855
Tensile	929	846
Tensile	940	857
Creep for 100 h then tensile	950	945
Creep for 200 h then tensile	959	956
500 cycles then tensile	917	860

for the stress calculations. The tensile strength and yield strength data are shown in Table 3. It can be seen that the prior creep at 815 MPa for 100 or 200 h increased both the tensile strength and the yield strength of the material. In contrast, prior fatigue loading for 500 cycles decreased the tensile strength and increased the yield strength slightly.

4.2. Effects of prior creep on fatigue behavior

To study the effect of prior creep on the fatigue life, we plotted the conventional fatigue life of the specimens after they had been subjected to prior creep for different times (see Fig. 15(a)). Herein, the stress was calculated based on the initial diameter of the test section of the specimens. It can be seen that for the same maximum stress as calculated based on the initial diameter of the test section of the specimens, the prior creep lowered the fatigue life of the specimens. In addition, the fatigue life decreased with an increase in the prior-creep time.

Fig. 15(b) shows the ratio of the diameter of the test section of specimens after they had been subjected to prior creep to that before this process. It can be seen that the diameter of the specimens after being subjected to creep is smaller than that before it. Furthermore, the post-creep diameter decreases with an increase in the prior-creep time.

Fig. 15(c) shows the variations in the fatigue life with the maximum stress as calculated based on the diameter of the test section of specimens after they had been subjected to creep, which is compared with the results for the specimens not subjected to prior creep. It can be seen that the prior creep either improved or reduced the fatigue resistance of the material. This phenomenon is related to the prior-creep time (i.e., the accumulation of plastic strain). Once the amount of prior plastic strain accumulated reaches a value that favors the crack initiation and growth, the fatigue life is lowered.

Fig. 15(d) shows the variations in the cumulative maximum and minimum strains with the number of loading cycles for the specimens subjected to prior creep and fracture within the extensometer. The prior-creep stress was 815 MPa and the maximum stress during the subsequent fatigue loading was 815 MPa, as calculated based on the initial diameter of the test sections of the specimens. It can be seen that the prior-creep time had little effect on the variations in the cumulative maximum and minimum strains with the number of loading cycles for the specimens subjected to prior-creep. Fig. 15(d) shows that the cumulative maximum strain for the specimens subjected to prior creep increased slowly with the number of loading cycles, in contrast to the case for the specimens not subjected to prior creep after the initial tens of cycles. Further, the cumulative maximum strain was lower than that for the specimens not subjected to prior creep after a certain number of cycles (270, 260, and 310 cycles for prior creep for 10 h, 100 h, and 200 h, respectively).

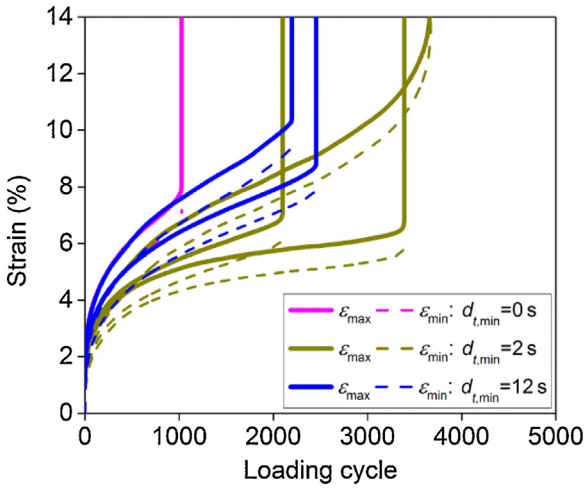

Fig. 10. Variations in cumulative maximum strain (ε_{max}) and minimum strain (ε_{min}) with number of loading cycles for specimens fractured within extensometer during dwell fatigue tests performed at σ_{max}=815 MPa, σ_{min}=0 MPa, and $d_{t,max}$ = 120 s.

For all three specimens subjected to prior creep for 10 h (Fig. 15(c)), the cumulative strain after prior creep for 10 h and that immediately after complete unloading after prior creep for 10 h are shown in Table 4. The experiments were performed on the MTS Landmark machine, and the strain was measured with an extensometer during the fatigue tests. The difference between the cumulative strain after prior creep for 10 h and that immediately after complete unloading is attributable to the recovery of the elastic strain. It can be seen from Table 4 that the cumulative plastic strain (i.e., the strain immediately after complete unloading subsequent to prior creep for 10 h) for the specimens subjected to prior creep for 10 h is greater than the cumulative maximum strain of the

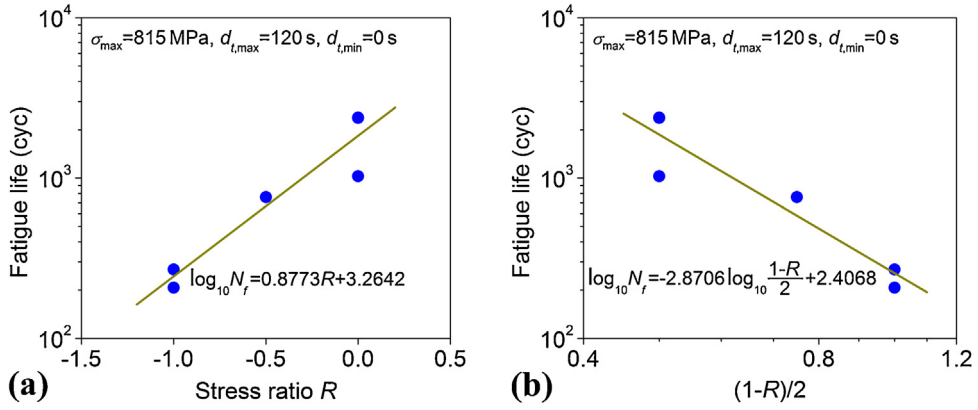

Fig. 11. Dwell fatigue life at different stress ratios R. Lines denote linear regression results. (a) Fatigue life versus R and (b) fatigue life versus (1–R)/2.

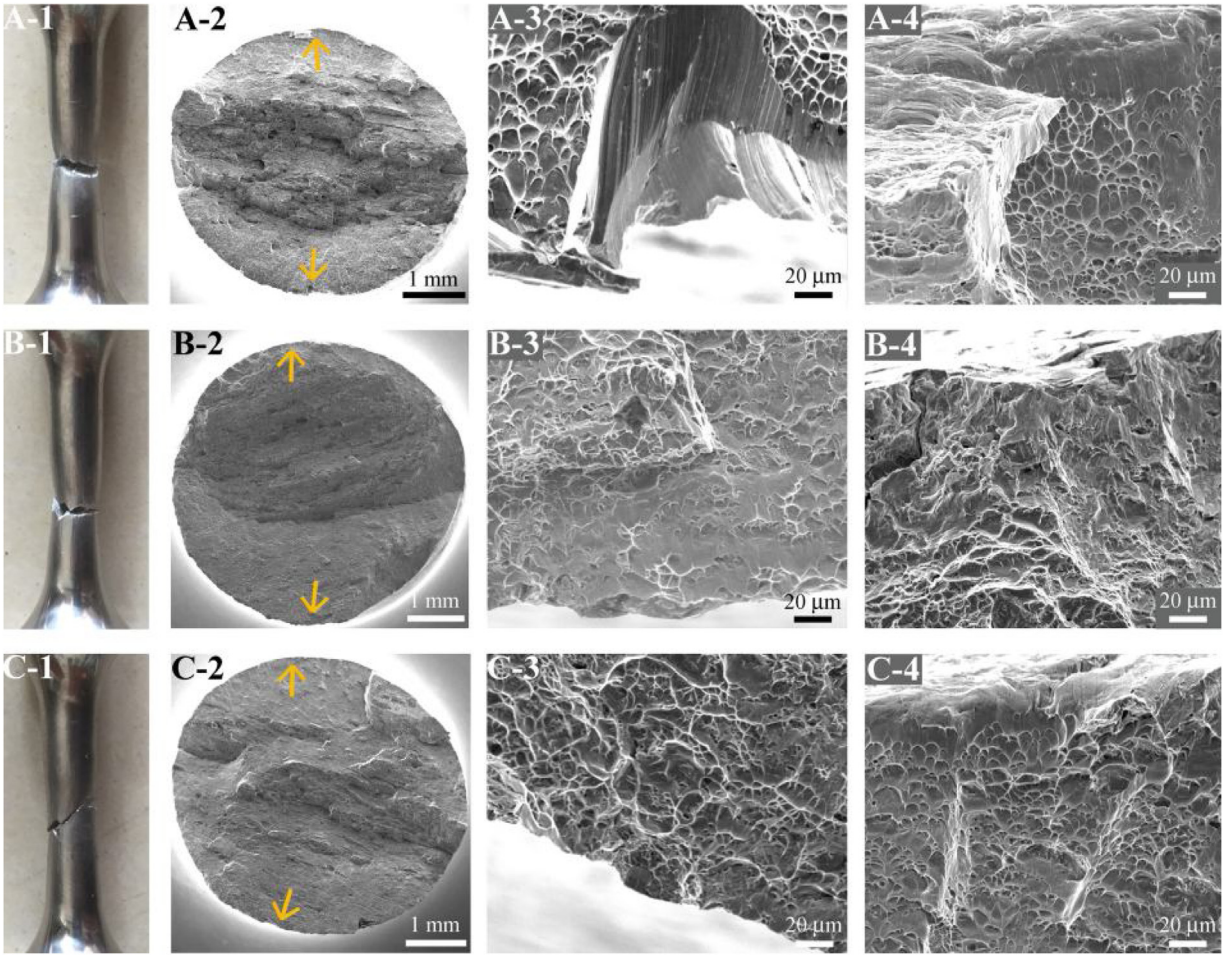

Fig. 12. Photographs and fracture surface morphologies of failed specimens subjected to dwell fatigue tests at negative stress ratios. A-1 to A-4: σ_{max}=815 MPa, $d_{t,max}$ = 120 s, σ_{min}=−815 MPa, $d_{t,min}$ = 0 s, and N_f = 207 cycles; A-1 is photograph of fractured specimen, A-2 is SEM image of fracture surface, and A-3 and A-4 are magnified images of regions corresponding to up and down arrows in A-2, respectively. B-1 to B-4: σ_{max}=815 MPa, $d_{t,max}$ = 120 s, σ_{min}=−815 MPa, $d_{t,min}$ = 0 s, and N_f = 269 cycles; B-1 is photograph of fractured specimen, B-2 is SEM image of fracture surface, and B-3 and B-4 are magnified images of regions corresponding to up and down arrows in B-2, respectively; C-1 to C-4: σ_{max}=815 MPa, $d_{t,max}$ = 120 s, σ_{min}=−407.5 MPa, $d_{t,min}$ = 0 s, and N_f = 761 cycles, C-1 is photograph of fractured specimen, C-2 is SEM image of fracture surface, and C-3 and C-4 are magnified images of regions corresponding to up and down arrows in C-2, respectively.

Table 4
Cumulative strains after prior creep for 10 h and immediately after complete unloading after prior creep for 10 h for specimens subjected to prior creep for 10 h.

Specimen No.	After prior creep for 10 h	Immediately after complete unloading after prior creep for 10 h
1	3.45%	2.68 %
2	3.69%	2.96 %
3	3.83%	3.08 %

specimen not subjected to prior creep as determined a few cycles before specimen failure. Hence, the actual cumulative maximum strain during loading (i.e., the cumulative plastic strain caused by prior creep plus the cumulative maximum strain owing to loading during the subsequent fatigue test) is greater than that of the specimen not subjected to prior creep. This indicates that for the same maximum stress as calculated based on the initial diameter of the test section of the specimens, the actual stress (i.e., the stress calculated based on the diameter of the test section of the specimens during each cycle) for each loading cycle for the specimens subjected to prior creep for 10 h, 100 h, and 200 h in Fig. 15 was greater than that of the specimen not subjected to prior creep over the entire fatigue test. In other words, the increase in the actual stress due to the decrease in the diameter of the test section of the specimens owing to prior creep is responsible for the decrease in the fatigue life of the specimens subjected to prior creep.

4.3. Interaction between dwell loading and fatigue loading

4.3.1. Effect of fatigue loading on creep behavior

The dwell fatigue of specimens at R = 0 resulted in fatigue failure, ductile failure and mixed failure, as stated in Section 3.1.2. For the specimens that exhibited ductile failure, it is more appropriate to consider the interaction between dwell loading and fatigue loading based on the effect of fatigue loading on the creep behavior. Fig. 16 shows a comparison of the cumulative maximum strain as a function of the loading time (i.e., cumulative test time) for the specimens that fractured within the extensometer during the dwell fatigue tests with that during the creep tests. The specimen with a dwell fatigue life N_f = 3669 cycles exhibited ductile failure, while the others exhibited fatigue failure or mixed failure. It can be seen from Fig. 16 that the cumulative maximum strain during the dwell fatigue tests is greater than the strain during the creep tests after a certain loading time. Moreover, the cumulative maximum strain during the dwell fatigue tests generally increased faster than the strain during the creep tests. This implies that a part of the fatigue loading process (i.e., the unloading and loading process) favors the increase in the plastic strain during dwell loading.

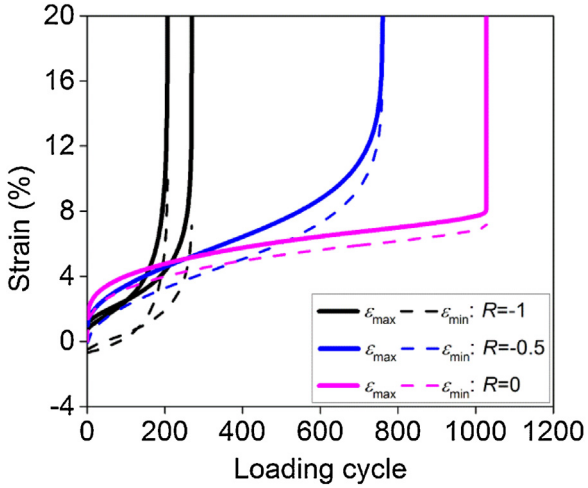

Fig. 13. Variations in cumulative maximum strain (ε_{max}) and minimum strain (ε_{min}) with number of loading cycles for dwell-fatigued specimens fractured within extensometer at σ_{max}=815 MPa, $d_{t,max}$ = 120 s, and $d_{t,min}$ = 0 and different stress ratios.

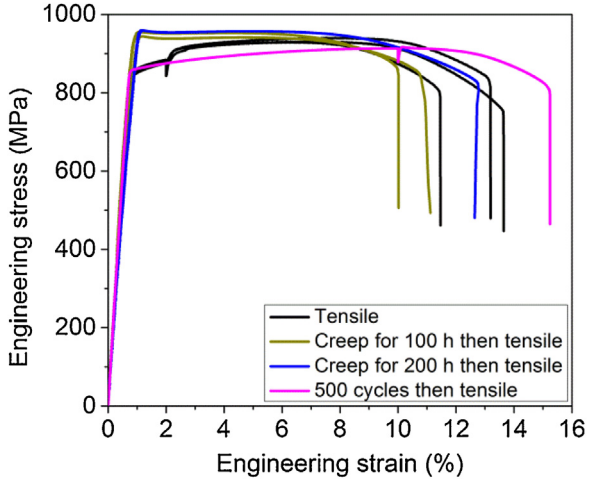

Fig. 14. Effects of prior creep and fatigue loading on tensile behavior. Prior-creep stress is 815 MPa and fatigue loading is σ_{max}=815 MPa, $d_{t,max}$ = 0 s, σ_{min} = 0, and $d_{t,min}$ = 0.

Fig. 16 also indicates that the loading time to failure under creep for the investigated Ti-6Al-4 V ELI alloy is much longer than that for dwell fatigue at the stress ratio R = 0. The loading time to failure for all the 11 specimens listed in Table 1 is less than 200 h. Further, the cumulative maximum strains of the failed specimens just before fracture are different. For the total of 11 specimens subjected to dwell fatigue test at R = 0, the strain was measured for 10 specimens during the dwell fatigue tests. Only 1 of the 10 tested specimens exhibited a cumulative maximum strain before fracture that was smaller than 6.91 % at 2515 h during the creep test for a constant tensile stress of 815 MPa. The cumulative maximum strain for this specimen was 6.79 % just before fracture, and the associated dwell fatigue life was N_f = 3391 cycles. This indicates that the cumulative maximum strain a few cycles before fracture cannot be used for evaluating the dwell fatigue life of titanium alloys. It should be

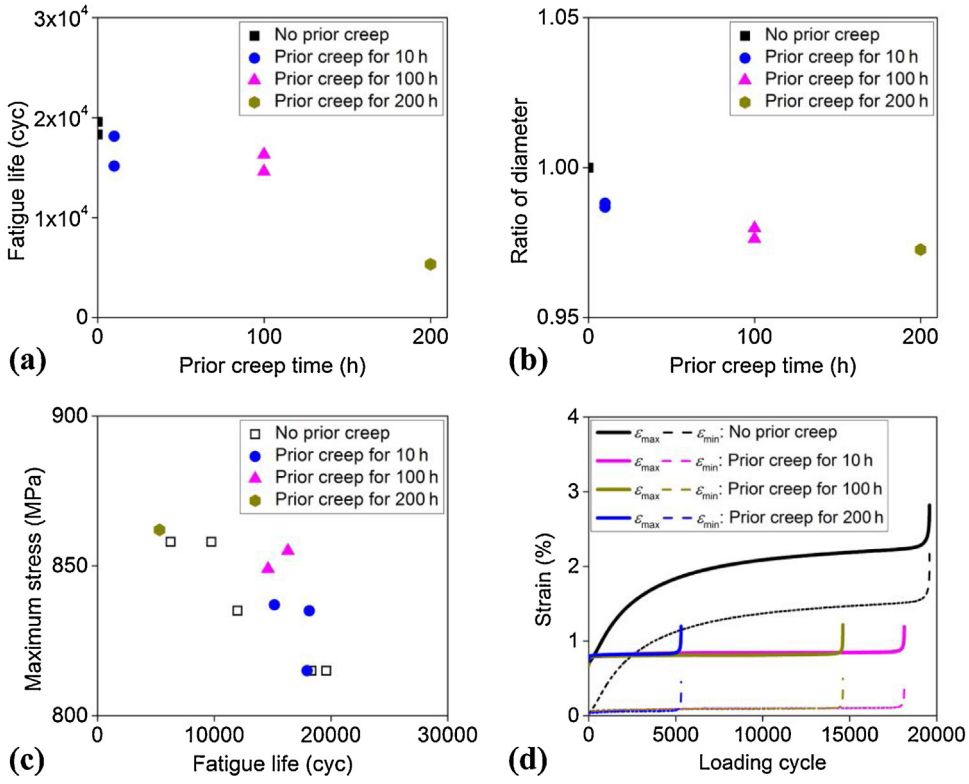

Fig. 15. Effect of prior creep on conventional fatigue life, diameter of test section of specimens, and cumulative strain as function of number of loading cycles. (a) Fatigue life versus prior creep time; prior-creep stress is 815 MPa as calculated based on initial diameter of test section of specimens, subsequent fatigue loading is σ_{max}=815 MPa, $d_{t,max}$ = 0 s, σ_{min} = 0, $d_{t,min}$ = 0, and maximum stress for fatigue loading was calculated based on initial diameter of test section of specimens. (b) Ratio of diameter of test section of specimens after prior creep to that before prior creep in (a). (c) Maximum stress versus fatigue life. Here, prior-creep stress is 815 MPa as calculated based on initial diameter of test section of specimens, and maximum stress during subsequent fatigue loading was calculated based on diameter of test section of specimens after being subjected to prior-creep. (d) Cumulative maximum strain (ε_{max}) and minimum strain (ε_{min}) versus number of loading cycles for prior-creep specimens fractured within extensometer. Herein, prior-creep stress is 815 MPa as calculated based on initial diameter of test section of specimens, and maximum stress during subsequent fatigue loading is 815 MPa as calculated based on initial diameter of test section of specimens.

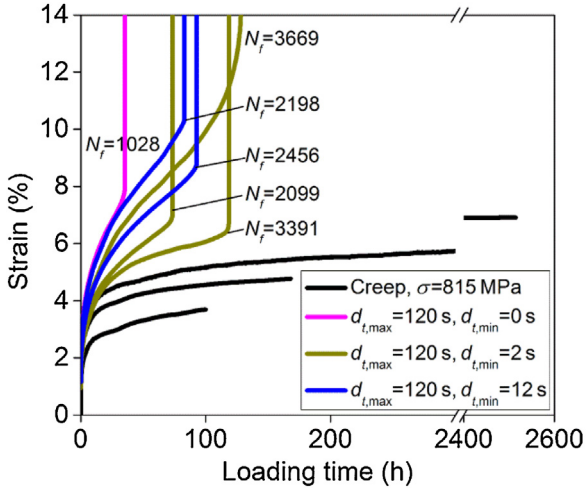

Fig. 16. Variations in cumulative maximum strain with loading time for specimens fractured within extensometer during dwell fatigue test with σ_{max}=815 MPa and σ_{min}=0 MPa. Results for creep tests are shown for comparison. The stress for creep tests is calculated based on initial diameter of test section of specimens.

noted that all the specimens in Fig. 16 are not failed during the creep tests.

4.3.2. Effect of dwell loading on fatigue behavior

Fig. 17 shows the effect of dwell loading on the cumulative maximum strain for the specimens that fractured within the extensometer, in which the plastic strain owing to the prior creep is involved for the specimen that subjected to prior creep for 200 h and then fatigue (see Fig. 17(a)). The plastic strain due to the prior creep was taken as 4.77 %, which was obtained from the cumulative strain (5.52 %) of the specimen at 200 h for the creep specimen (see Fig. 16) minus the average value of the elastic strain recovery (0.75 %) in Table 4. It can be seen from Fig. 17 that the cumulative maximum strain increases with an increase in the number of loading cycles and loading time (i.e., the cumulative test time) for both continuous dwell fatigue and intermittent dwell fatigue. For the same number of loading cycles or loading time before specimen failure, the cumulative maximum strains under continuous fatigue loading and intermittent fatigue loading are both smaller and increase more slowly than those under continuous dwell fatigue and intermittent dwell fatigue.

Further, Fig. 17(a) shows that the effect of dwell loading on the cumulative maximum strain is significantly dependent on the form in which dwell loading is introduced. For the fatigue of the specimens subjected to prior dwell loading, the cumulative maximum strain is greater than the dwell fatigue during the initial cycles. It then becomes smaller than the dwell fatigue. The variation in the cumulative strain with the number of loading cycles is exceedingly small after the initial few cycles of fatigue loading for the specimens subjected to prior dwell loading. In contrast, the cumulative maximum strain increases with the number of loading cycles during the entire dwell fatigue loading process (i.e., repeated dwell loading and fatigue loading).

Fig. 17 shows that the part of the dwell load during the dwell fatigue process leads to an increase in the actual stress of the test section of the specimens. This is due to the increase in the transverse shrinkage induced by the dwell load during the dwell fatigue process. Macroscopically, for the same stress ratio, a higher maximum stress results in a lower fatigue life. Thus, the increase in the actual stress (i.e., the decrease in the diameter) of the test section of the specimens owing to the increase in the plastic strain because of dwell loading during the dwell fatigue test is one of primary factors responsible for the dwell fatigue life being lower than the conventional fatigue life. Microcosmicly, the increase in the plastic strain aids the growth of crack or damage. Because of these two factors, the fatigue life during the dwell fatigue process with the maximum stress dwell is lower than the conventional fatigue under other identical conditions.

In addition, for the specimens subjected to dwell fatigue at $R = 0$ (see Table 1), the cumulative dwell loading time (the dwell loading time multiplies by the fatigue life) is less than 170 h. Moreover, for 8 of the 11 specimens, it is less than 100 h. It can be seen from Fig. 15(a) that when the maximum load for the subsequent fatigue test is the same as the prior dwell load (i.e., creep load), the higher the dwell loading (i.e., creep) time, the lower the fatigue life of the specimens will be after they are subjected to prior dwell loading. The fatigue life of the specimens after being subjected to prior creep for 200 h is 5316 cycles, which is longer than the dwell fatigue lives of the specimens listed in Table 1. This indicates that for the dwell loading conditions used in this study, the fatigue life of the specimens after being subjected to prior creep is longer than their dwell fatigue life when the prior-creep time is equal to the cumulative dwell loading time for the specimens during the dwell fatigue process.

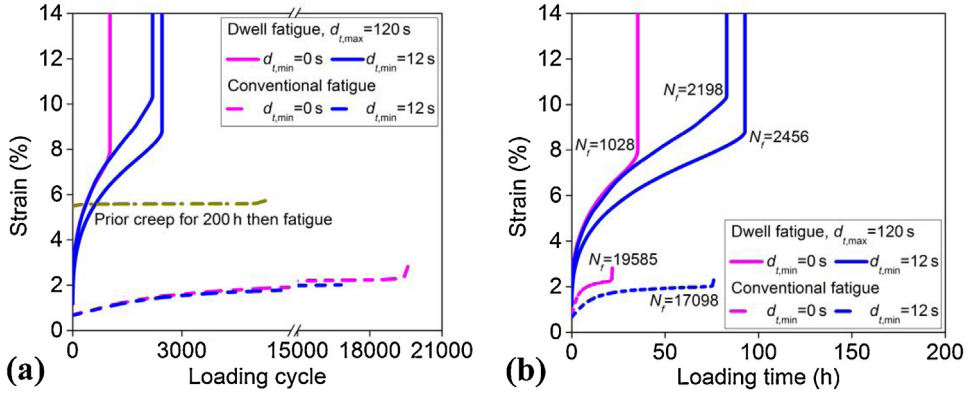

Fig. 17. Effects of dwell loading and prior creep on cumulative maximum strain of specimens fractured within extensometer. (a) Cumulative maximum strain versus number of loading cycles, σ_{max}=815 MPa and σ_{min}=0 MPa. Specimens subjected to prior creep for 200 h at σ =815 MPa exhibited plastic strain because of creep and then fatigue. The stress for prior creep is calculated based on initial diameter of test section of the specimen. (b) Cumulative maximum strain versus loading time, σ_{max}=815 MPa and σ_{min}=0 MPa.

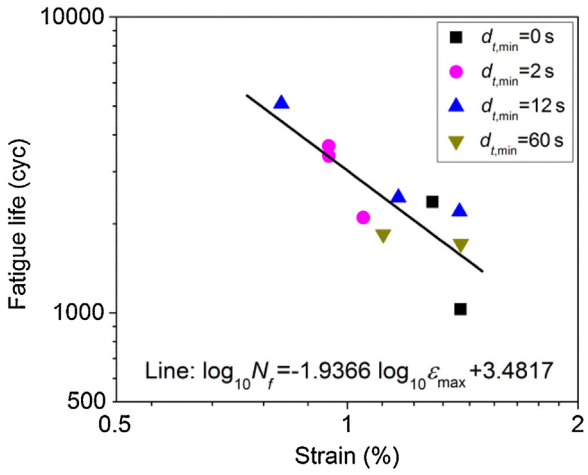

Fig. 18. Fatigue life versus cumulative maximum strain (ε_{max}) during first loading cycle of dwell fatigue test. Line denotes linear regression result for dwell fatigue life (N_f) on logarithmic scale and strain (ε_{max}) on logarithmic scale.

4.4. Mechanism of dwell fatigue

The results in Section 4.3 indicate that the interaction between dwell loading and fatigue loading accelerates the failure of the specimens than that when they are subjected to only dwell loading or fatigue loading. On the one hand, the increase in the plastic strain caused by the part of dwell load during the dwell fatigue process leads to an increase in the actual stress of the test section of the specimens during the subsequent loading cycles. Moreover, it aids the growth of the formed crack or damage during the dwell fatigue process. This is in accordance with the result that the effect of dwell loading on the fatigue life is reduced with a decrease in the dwell stress and disappears in the case of a relatively lower maximum stress dwell [10]. On the other hand, the accumulation of local plastic strain or the damage caused by the part of the fatigue load during the dwell fatigue process increases the cumulative plastic strain than that for individual creep (see Section 4.3.1). The interaction between dwell loading and fatigue loading results in a competition between the different failure modes. This agrees with the SEM observations of the fracture surfaces of the specimens subjected to dwell fatigue. When fatigue crack initiation and propagation are dominant, fatigue failure occurs. When the cumulative plastic strain is dominant, ductile failure occurs.

4.5. Evaluation of dwell fatigue life

Next, we tried to correlate the dwell fatigue life to the strain during the dwell fatigue process. It was found that the specimens with a higher cumulative maximum strain during the first loading cycle exhibited a lower dwell fatigue life for the same intermittent loading time, as shown in Fig. 18. We had shown in Section 3.1.1 that the intermittent loading time has a negligible effect on the dwell fatigue life. In the absence of the intermittent loading time, the dwell fatigue life tends to decrease with an increase in the cumulative maximum strain during the first loading cycle. Further, it was found that the dwell fatigue life and the cumulative maximum strain during the first loading cycle exhibit an approximately linear relationship on the log–log scale, as shown in Fig. 18. The correlation coefficient is –0.832, indicating that the correlation is highly significant [30]. This indicates that the dwell fatigue performance of materials can be evaluated based on their cumulative maximum strain during the first loading cycle.

5. Conclusions

In this study, experimental investigations and theoretical analyses were performed to elucidate the effects of intermittent loading time and stress ratio on the dwell fatigue behavior of the titanium alloy Ti-6Al-4 V ELI, which could be used for the pressure hull of deep-sea submersibles. The primary results of the study are as follows:

(1) The intermittent loading time has no effect on the dwell fatigue life and dwell fatigue failure mechanism of the investigated Ti-6Al-4 V ELI alloy, in contrast to its effect on the conventional fatigue behavior. In the case of conventional fatigue, intermittent loading has an adverse effect on the fatigue life and tends to induce multiple crack initiation. The dwell fatigue failure modes of the investigated Ti-6Al-4 V ELI alloy could be classified into three types: i) fatigue failure mode, ii) ductile failure mode, and iii) mixed failure mode.
(2) The stress ratio has a significant effect on the fatigue life and dwell fatigue mechanism. The dwell fatigue life increases with an increase in the stress ratio for the same maximum stress. Moreover, the dwell fatigue life on the logarithmic scale is linearly related to the stress ratio R or $(1–R)/2$ on the logarithmic scale. The specimens at a negative stress ratio exhibited ductile failure.
(3) The mechanism of dwell fatigue in titanium alloys is related to the following factors: (i) the increase in the plastic strain caused by the part of the dwell load leads to an increase in the actual stress of the test section of the specimens during the subsequent loading cycles and aids the growth of the formed crack or damage during the dwell fatigue process. (ii) The local plastic strain or damage induced by the part of the fatigue load increases the cumulative plastic strain as compared with the case for individual creep. The interaction between dwell loading and fatigue loading accelerates the failure of the specimens as compared with the case for creep or fatigue loading alone. This is in agreement with the experimental results obtained for the investigated Ti-6Al-4 V ELI alloy.
(4) The dwell fatigue life tends to decrease with an increase in the cumulative maximum strain during the first loading cycle for the investigated loading conditions for the Ti-6Al-4 V ELI alloy. This could be modeled by a linear relationship on the log–log scale and can be used to evaluate the dwell fatigue life with the maximum stress dwell.

The results obtained in this study will be helpful for our understanding of the dwell fatigue behavior of titanium alloys and for the evaluation of dwell fatigue life of the pressure hulls of deep-sea submersibles made of titanium alloys.

Declaration of Competing Interest

The authors declare that they have no known competing financial interests or personal relationships that could have appeared to influence the work reported in this paper.

Acknowledgements

This work was financially supported by the National Key Research and Development Program of China (No. 2017YFC0305500).

References

[1] Z. Song, D.W. Hoeppner, Int. J. Fatigue 10 (1988) 211–218.
[2] M.R. Bache, Int. J. Fatigue 25 (2003) 1079–1087.

[3] P. Lefranc, V. Doquet, M. Gerland, C. Sarrazin-Baudoux, Acta Mater. 56 (2008) 4450–4457.
[4] J. Qiu, Y. Ma, J. Lei, Y. Liu, A. Huang, D. Rugg, R. Yang, Metall. Mater. Trans. A 45 (2014) 6075–6087.
[5] S. Waheed, Z. Zheng, D.S. Balint, F.P.E. Dunne, Acta Mater. 162 (2019) 136–148.
[6] Q. Song, Y. Li, L. Wang, R. Huang, C. Sun, Metals 9 (2019) 914.
[7] V. Sinha, M.J. Mills, J.C. Williams, Metall. Mater. Trans. A 35 (2004) 3141–3148.
[8] C. Lavogiez, S. Hémery, P. Villechaise,Int. J. Fatigue 131 (2020), 105341.
[9] W.J. Evans, C.R. Gostelow, Metall. Trans. A 10 (1979) 1837–1846.
[10] M.R. Bache, M. Cope, H.M. Davies, W.J. Evans, G. Harrison, Int. J. Fatigue 19 (1997) S83–S88.
[11] F. Wang, W. Cui, Mater. Sci. Eng. A 642 (2015) 136–141.
[12] P.J. Bania, D. Eylon, Metall. Trans. A 9 (1978) 847–855.
[13] D. Munz, V. Bachmann, Materialwiss. Werkst. 11 (1980) 168–172.
[14] W. Shen, W.O. Soboyejo, A.B.O. Soboyejo, Mech. Mater. 36 (2004) 117–140.
[15] Y. Li, C. Bian, K. Wang, X. Sun, C. Qin, J. Ship Mech. 22 (2018) 1124–1135.
[16] M.T. Whittaker, W.J. Evans, W. Harrison, in: Icf12 Ottawa (2013).
[17] W.J. Evans, Fatigue Fract. Eng. Mater. Struct. 27 (2004) 543–557.
[18] W.J. Evans, M.R. Bache, Int. J. Fatigue 16 (1994) 443–452.
[19] L. Yang, J. Liu, J. Tan, Z. Chen, Q. Wang, R. Yang, J. Mater. Sci. Technol. 30 (2014) 706–709.
[20] M.E. Kassner, Y. Kosaka, J.S. Hall, Metall. Mater. Trans. A 30 (1999) 2383–2389.
[21] C.A. Stubbington, S. Pearson, Eng. Fract. Mech. 10 (1978) 723–756.
[22] W.J. Evans, J. Mater. Sci. Lett. 6 (1987) 571–574.
[23] W.J. Evans, M.R. Bache, Scr. Metall. Mater. 32 (1995) 1019–1024.
[24] J. Liu, L. Yang, Q. Wang, R. Yang, in: V. Venkatesh, A.L. Pilchak, J.E. Allison, S. Ankem, R. Boyer, J. Christodoulou, H.L. Fraser, M.A. Imam, Y. Kosaka, H.J. Rack, A. Chatterjee, A. Woodfield (Eds.), Proceedings of the 13th World Conference on Titanium, The Minerals, Metals & Materials Society, California, 2016, pp. 955–958.
[25] Z. Wu, H. Kou, N. Chen, M. Zhang, K. Hua, J. Fan, B. Tang, J. Li, J. Mater. Sci. Technol. 50 (2020) 204–214.
[26] Y. Li, Q. Song, S. Feng, C. Sun, Materials 11 (2018) 1628.
[27] Z. Zhang, L. Li, Z. Zhang, P. Zhang, J. Mater. Sci. Technol. 33 (2017) 603–606.
[28] Z. Zheng, D.S. Balint, F.P.E. Dunne, J. Mech. Phys. Solids 96 (2016) 411–427.
[29] R.J. Morrissey, D.L. McDowell, Int. J. Fatigue 21 (1999) 679–685.
[30] J.R. Taylor, An Introduction to Error Analysis, second ed., University Science Books, California, 1997.